ELSEVIER

Ceramics International 33 (2007) 49–58

CERAMICS INTERNATIONAL

www.elsevier.com/locate/ceramint

Enhancement of the physical properties of rare-earth-substituted Mn–Zn ferrites prepared by flash method

M.A. Ahmed [a,*], N. Okasha [b], M.M. El-Sayed [c]

[a] *Physics Department, Faculty of Science, Cairo University, Giza, Egypt*
[b] *Physics Department, Faculty of Girls, Ain Shams University, Cairo, Egypt*
[c] *Physics Department, Faculty of Education, Ain Shams University, Cairo, Egypt*

Received 14 March 2005; received in revised form 26 May 2005; accepted 6 July 2005
Available online 19 September 2005

Abstract

The effect of rare-earth ions on the structural, magnetic and electrical properties of rare-earth-doped manganese–zinc ferrite is reported. The compounds with the formula $Mn_{0.5}Zn_{0.5}R_{0.05}Fe_{1.95}O_4$ where R = Tb, La, Ce and Th, were prepared by the flash combustion technique. The prepared samples reveal that by introducing a relatively small amount of $R(NO_3)_3$ or $R(Cl_3)$ instead of Fe_2O_3, an important modification of both structure and physical properties was obtained. Curie temperature, effective magnetic moment, electrical resistivity, density, thermoelectric and lattice constant were directly affected by these substitutions either by their partial diffusion in the spinel lattice or the formation of the crystalline secondary phases (orthoferrite and/or garnet) on the grain boundaries which suppress the abnormal grain growth. Correlation between the ionic radii and the measured physical properties were studied.

Keywords: D. Ferrites; Flash method; Rare-earths substitutions; Physical properties of Mn–Zn ferrites

1. Introduction

Mn–Zn ferrites are ceramic ferromagnetic materials possessing excellent magnetic properties, such as high initial permeability and low magnetic losses. These physical properties vary depending on the preparation conditions such as sintering temperature, sintering time, rate of heating and cooling, etc. [1,2]. Thus, they are mainly used in industrial applications, such as the cores for inductors, transformers, recording heads and switch mode power supplies [3–6]. It is well known that manganese ferrite is inverse spinel because 80% of Mn^{3+} ions occupy A sites [7]. However, Mn^{3+} ions occupy the B site (octahedral) which depend on the presence of Fe^{2+} on this site where the exchange interaction takes place [8]. The cation distribution for Mn–Zn ferrite can be represented by $(Mn^{2+}_{0.8} + Fe^{3+}_{0.2})^A[Mn^{3+}_{0.2}Fe^{2+}_{0.2}Fe^{3+}_{1.6}]^BO_4$ where the carriers are created by the following reaction of electron exchange on octahedral site as the electron exchange takes place as $Mn^{2+} + Fe^{3+} \leftrightarrow Mn^{3+} + Fe^{2+}$. The result of this electron exchange is the extraordinarily small electrical conductivity as compared with the metals.

Introducing small amount of rare-earth oxides as impurity gives a disordered structure, causing the transition temperature to fall abruptly or disappear [9]. As the concentration of the ion substitution increases, thermally activated Fe^{2+} valency states result in an increase in the electrical conduction by hopping mechanism [10]. Phillips et al. [11] have proposed that the electrical conductivity of Li–Zn ferrite has been interpreted as depending on both nearest-neighbor hopping at high temperatures and on variable range hopping at low temperatures.

The study of the electrical resistivity produces valuable information on the behavior of free and localized electric charge carriers in the studied samples. In Mn–Zn ferrites, zinc volatilization at high temperatures results in the formation of Fe^{2+} ions thereby increasing hopping and reducing the resistivity of the sample [12].

* Corresponding author.
E-mail address: moala47@yahoo.com (M.A. Ahmed).

0272-8842/$30.00
doi:10.1016/j.ceramint.2005.07.014

The rare-earth oxides [13] are good electrical insulators and have resistivities at room temperature greater than 10^6 Ω cm [14]. In the case of advanced functional materials, doping with small concentration of different rare-earth (R^{3+}) ions is a well-known straightforward and versatile way to tune the desirable physical properties of ferrites not only because of the lanthanide contraction which induced monotonic change of ionic radii, but also because of the different stable oxidation states and the periodical variation in magnetic moments coming from the sequential filling of electrons in their 4f shells. Talanov [15] and Ciufarov and Vorobiev [16] reported that the possibility of formation of compounds with inverse spinel structure takes place when R^{3+} substitutes Fe^{3+} on the octahedral sites, similar to the case of Ca^{2+} ions in $NiFe_2O_4$ [17]. Besides, the magnetic behavior of the ferromagnetic materials is largely governed by Fe–Fe interaction (the spin coupling of the 3d electrons). If the R^{3+} ions enter the spinel lattice, the R–Fe interactions also appear (4f–3d coupling), which can lead to small changes in the magnetization and Curie temperature. The R–R interactions are very weak since they result from the indirect 4f–5d–4f mechanism [18].

The aim of the present work is to introduce a new era for improving the physical properties of rare-earth-doped Mn–Zn ferrite through the flash method of preparation which requires small time and low cost to obtain more applicable samples. This can be done through structural as well as magnetic and electrical properties investigations.

2. Experimental

The investigated samples have the formula $Mn_{0.5}Zn_{0.5}R_{0.05}Fe_{1.95}O_4$ where R = Tb, La, Ce and Th. The starting materials used $TbCl_3$, $La(NO_3)_3$, $Ce_2(SO_4)_3$, $Th(NO_3)_4$ and $Fe(NO_3)_3$ were of high purity (BDH) and urea. Flash combustion technique [19–21] was used where the chemicals were weighted according to the required stoichiometric proportion and mixed together for few minutes. Urea was added to the mixture and again well grounded. The mixture was transferred to Pt crucible and introduced into an electric furnace kept at presintering at 500 °C for 15 min. At this temperature, the mixture reacts giving out gases and the combustion was complete in 3–5 min. A foamy and highly porous precursor mass was obtained. It was collected and then powdered for further processing. The ferrite precursor powder was calcined at 900 °C for 2 h and made into pellets using uniaxial press of pressure 1.9×10^8 N/m^2. The compacted samples were sintered at a final temperature of 1340 °C for 3 h at a rate of 3 °C/min. The calcined ferrite powders were checked using XRD analysis model (Proker D8) with Cu Kα radiation and wavelength (λ = 1.5418 Å). The real part of dielectric constant (ε') and a.c. electrical resistivity were measured using bridge model (4275A Multi-Frequency LCR Meter, Hewlett Packard, USA) using the two-probe method [22] at different temperatures (300–800 K) as a function of the applied frequency ranged as (40 kHz–2 MHz). The d.c. magnetic susceptibility of the sample was measured using Faraday's method in which the sample was inserted in the point of maximum gradient. The measurements were performed over a temperature range where a paramagnetic behavior was observed in all the samples. The preparation steps by the flash method are shown in the flow chart.

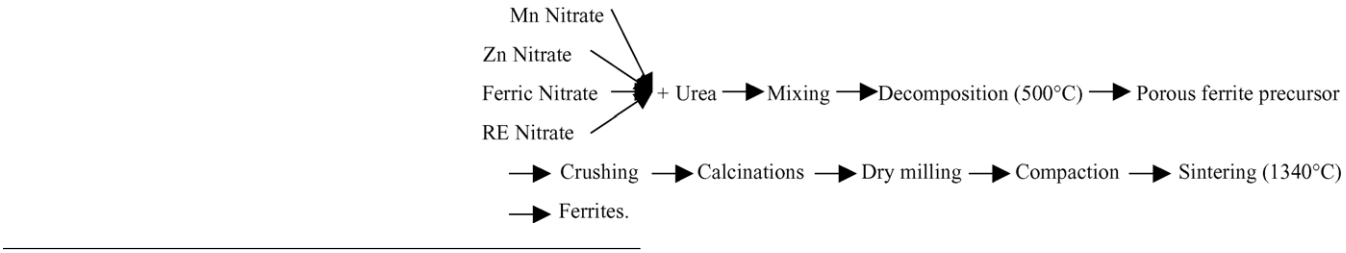

The temperature of the samples was measured using T-type thermocouple with an accuracy better than ±1 °C.

The thermoelectric power was also measured in order to know the type of charge carriers participating in conduction process.

3. Results and discussion

3.1. X-ray analysis

X-ray diffractograms (Fig. 1) show that the investigated samples have the single phase cubic spinel structure. Except for Mn–Zn ferrite (without substitution), another small peaks indicating the presence of secondary phase, which are identified by JCPDS card as orthoferrite ($RFeO_3$), is found. All the peaks in the pattern match well with the characteristic reflections of Mn–Zn ferrite reported earlier [23,24]. This means that the formation of secondary phases in the ferrite during sintering process is governed by the type and the amount of R^{3+} used. Therefore, the small amounts of R^{3+} ions in Mn–Zn ferrite can be affect not only the phase composition but also the size of the spinel matrix.

The lattice constant (a) and X-ray density (D_x) were computed, reported in Table 1 and shows in Fig. 2a and b.

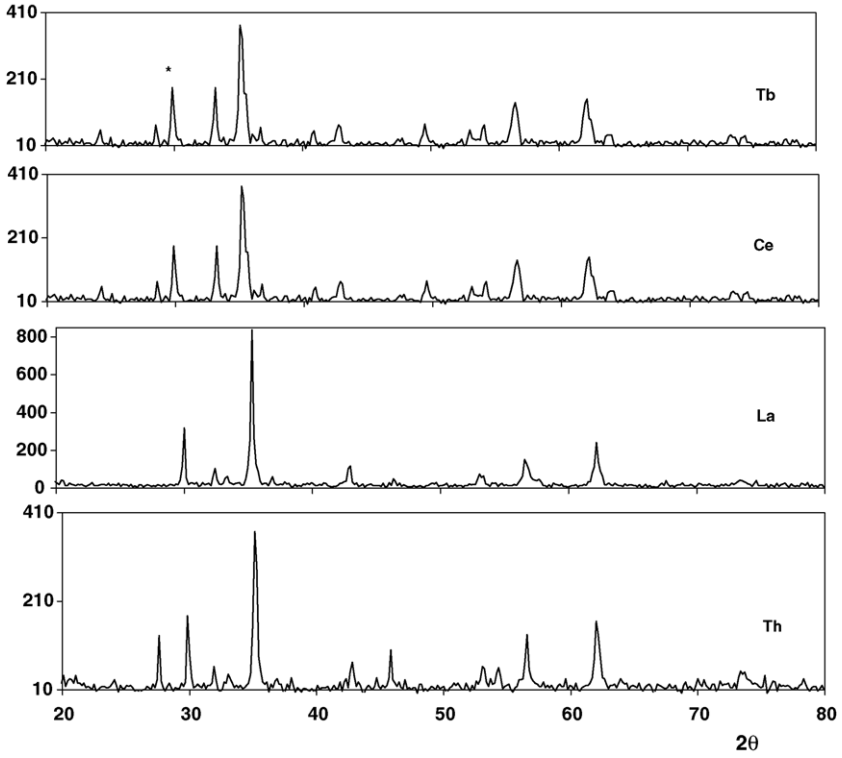

Fig. 1. X-ray diffraction patterns of $Mn_{0.5}Zn_{0.5}R_{0.05}Fe_{1.95}O_4$ where R = Tb, Ce, La, Th.

The samples are listed in order of increasing the ionic radius of R^{3+} ions. It is observed that, the values of (a) changes depending on R^{3+} radius. Fig. 2c shows the relation between the value of the full width at half maximum (FWHM) of (3 1 1) diffraction peak versus ionic radius of R^{3+} ions. The figure confirmed that doping with R^{3+} ions could restrain grain crystallization during sintering process.

3.2. Magnetic properties

It is known that [25] the magnetic behavior of Mn–Zn ferrite is governed by the iron–iron interaction (the spin coupling of the 3d electrons). Generally, an evaluation of this interaction can be obtained by analyzing the Curie temperature or the magnetization. The effect of partial substitution of iron by rare-earth ions on the molar magnetic susceptibility χ_M versus absolute temperature ranging from 300 to 800 K as a function of magnetic field intensity (720, 1020 and 1470 Oe) is shown in Fig. 3a–e. From the figure it is clear that the ferrimagnetic behavior can be observed for all samples and almost independent of the type of R ion. The values of χ_M are smaller than those of pure Mn–Zn ferrite. This can be explained due to some proposed, such as the R^{3+} ions enter only partially into the spinel lattice and the rest form with Fe^{3+} ions secondary phases besides, the R^{3+} ions on B sites behave paramagnetically; the magnetic ions distribution differs from that of Mn–Zn ferrite without R^{3+} ions.

Fig. 4a indicates the dependence of the Curie temperature T_C on the ionic radius of the rare-earth elements. The result shows that, the R^{3+} substitution increases the Curie temperature of Mn–Zn ferrite. This behavior is due to the replacement of R on the expense of Fe ions, as the result of the modification of the A–B exchange interaction strength. Besides, the increase of T_C for R-substituted specimens indicates that in these materials the negative Fe–Fe interaction is the strongest one and R–Fe interaction (4f–3d coupling) has a minor influence at high temperatures

Table 1
Chemical composition, lattice constant (a), X-ray density (D_x) and FWHM value of (3 1 1) diffraction peak of $Mn_{0.5}Zn_{0.5}R_{0.05}Fe_{1.95}O_4$

Sample	Chemical composition	Secondary phases	a (Å)	D_x (g/cm^3)	FWHM
None	$Mn_{0.5}Zn_{0.5}F_2O_4$	–	8.5031	5.06	5.95
Tb	$Mn_{0.5}Zn_{0.5}Tb_{0.05}Fe_{1.95}O_4$	$TbFeO_3$ (orthoferrite)	8.4511	5.27	5.9
Ce	$Mn_{0.5}Zn_{0.5}Ce_{0.05}Fe_{1.95}O_4$	CeO_2	8.4464	5.25	6.15
La	$Mn_{0.5}Zn_{0.5}La_{0.05}Fe_{1.95}O_4$	$LaFeO_3$ (orthoferrite)	8.388	5.28	6.05
Th	$Mn_{0.5}Zn_{0.5}Th_{0.05}Fe_{1.95}O_4$	ThO_2	8.4497	5.35	6.15

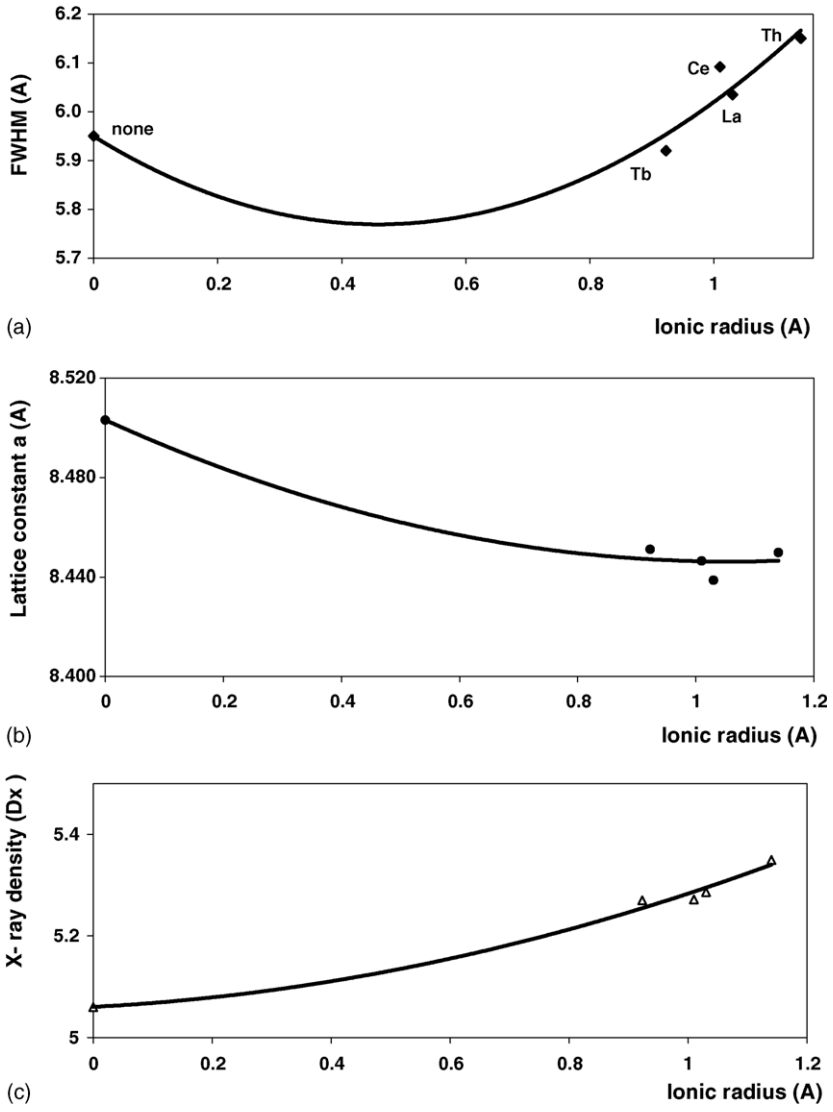

Fig. 2. (a–c) The change of full width at half maximum (FWHM), lattice constant (a) and X-ray density (D_x) as a function of ionic radius of R^{3+} ion used.

[26–30]. The observed variation in the Curie temperature may be explained on the basis of the exchange interactions. As the exchange interactions between the magnetic ions in A and B sublattices increase with both the density and the magnetic moment of the magnetic ions, greater amount of thermal energy is required to off set the effects of exchange interactions. When Fe^{3+} ions are replaced by magnetic Mn^{3+} ions, the magnetic moment of A sublattices will be reduced due to the reaction $Fe^{3+} + Mn^{2+} \leftrightarrow Fe^{2+} + Mn^{3+}$ as mentioned before and net magnetic moment increases. Consequently, the Curie temperature increases.

Fig. 4b shows the effect of different ionic radius (r) on the exchange interaction (J). It is observed that it reveals an increase in the value of J with the substitution of R^{3+} ions. It is therefore concluded that the substitution of R^{3+} ions in Mn–Zn ferrites support the magnetic properties of these samples.

Fig. 5a and b illustrated the relation between the values of magnetic susceptibility and the ionic radius of R^{3+} ions as a function of magnetic field intensity. The magnetic susceptibility decreases with increasing the magnetic field intensity as mentioned before due to the interaction between A and B sites. The dependence of the values of effective magnetic moment (μ_{eff}) on magnetic field intensity (H) as a function of ionic radius is presented graphically in Fig. 5b. From this figure, it is clear that a decrease in the effective magnetic moment with increasing (H) is consistent with the strengthening of A–B interaction due to the replacement of Mn^{3+} on expense of Fe^{3+} on octahedral sites, which results in an increase of magnetization of B sites and reduction in magnetization of A sites. This reduces the B–B interaction and A–B interaction starts to increase. Besides, the replacement of RE^{3+} ions with smaller ionic radius on Fe^{3+} in octahedral sites affect on the A–B exchange interaction leading to decrease in μ_{eff}. The values of

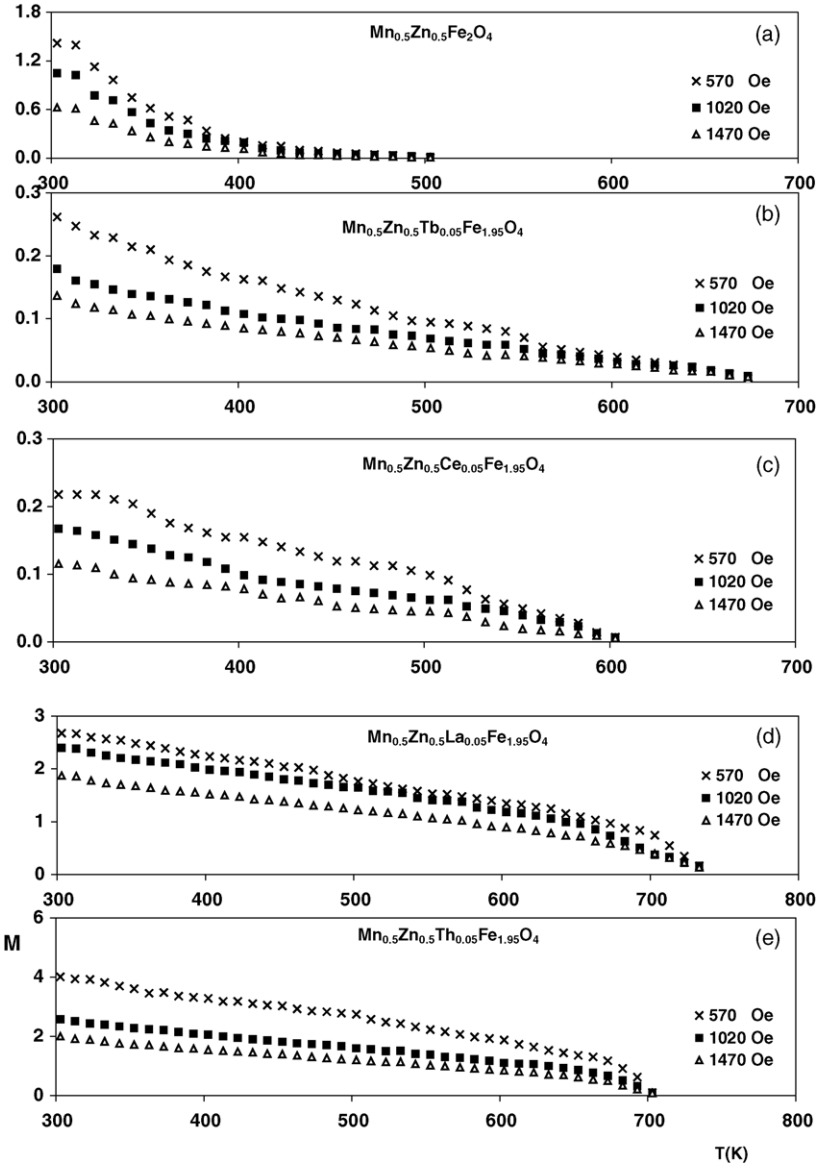

Fig. 3. (a–e) Temperature dependence of the molar magnetic susceptibility (χ_M) at different magnetic field intensity (H).

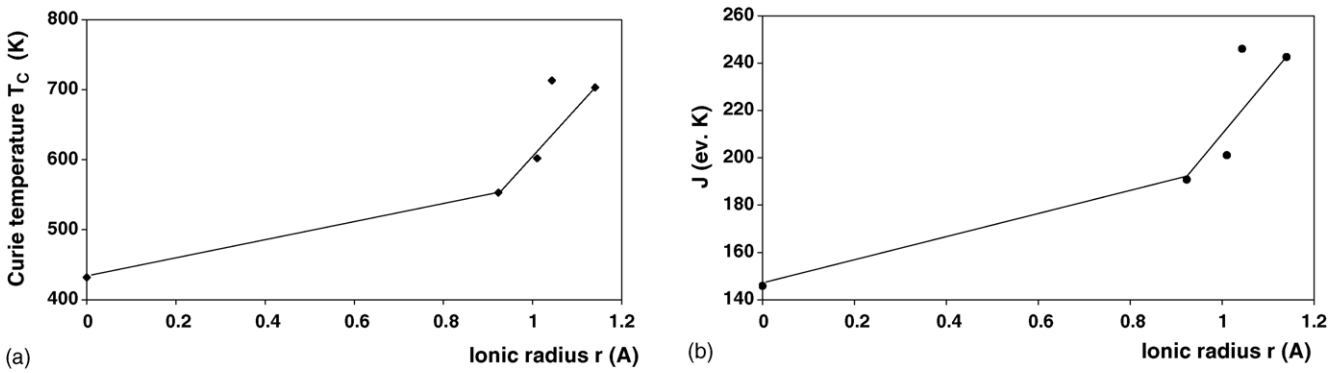

Fig. 4. (a) The Curie temperature as a function of ionic radius of rare-earth ion; and (b) the effect of ionic radius on the exchange interaction (J).

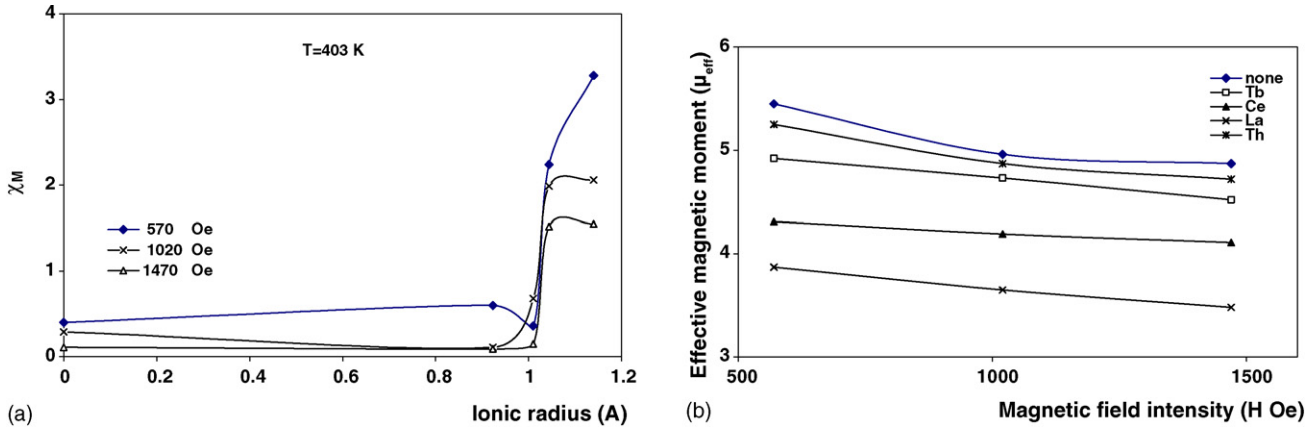

Fig. 5. (a) The change of magnetic susceptibility as a function of ionic radius; and (b) the relation between the effective magnetic moment and magnetic field intensity.

effective magnetic moment μ_{eff}, Curie temperature T_C and the molecular field constant λ are listed in Table 2 where λ calculated using the formula $T_C = \lambda \times C$; C is the Curie constant.

3.3. Electrical properties

Fig. 6a–c is a typical curve showing the influence of the R^{3+} ions on the dependence of the dielectric constant (ε') on

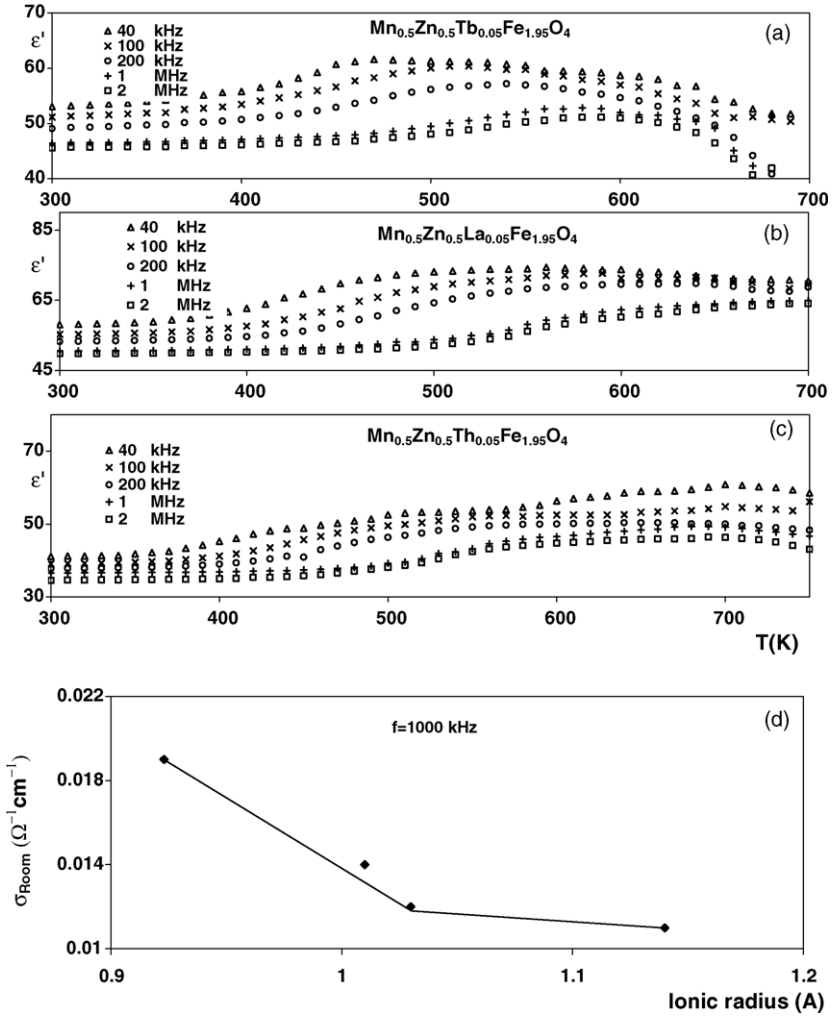

Fig. 6. (a–d): Temperature dependence of ε' at different frequency ranging from 40 kHz to 2 MHz. (d) The effect of ionic radius (r) on σ at room temperature.

Table 2
Effective magnetic moment (μ_{eff}) in (B M.), Curie temperature (T_C), exchange interaction constant (J) and molecular field constant (λ) of $Mn_{0.5}Zn_{0.5}R_{0.05}Fe_{1.95}O_4$

Sample	μ_{eff}			T_C (K)	J	λ
	570 Oe	1020 Oe	1470 Oe			
None	5.45	4.79	4.37	550	189.75	148.25
Tb	4.2	4.12	3.92	530	182.85	253.59
Ce	4.87	4.65	4.48	510	175.95	172.29
La	3.31	3.19	3.28	500	172.50	416.67
Th	5.6	4.92	4.72	475	163.88	213.97

the absolute temperature as a function of the applied frequency from 40 kHz to 2 MHz. It is evident that by increasing the temperature, the dielectric constant increases gradually up to the particular point designated as the dielectric transition temperature (T_d). Beyond this temperature, the values of dielectric constant for all samples were found to decrease. Similar behavior has been reported earlier [31,32]. Besides, the transition temperature (T_d) is shifted with increasing frequency. This behavior can be explained on the basis of the polarization effects. The space–charge polarization either between the surface of the sample and the electrodes or in the bulk of the material is governed by the number of the charge carriers as a result of increasing the temperature which is related to the hopping conduction mechanism in all the samples due to the electron exchange between Fe^{2+} and Fe^{3+} ions on the octahedral sites which is responsible on the dielectric properties [33]. Moreover, the exchange jumping of electrons between Fe^{2+} and Mn^{3+} with increasing temperature causes a local displacement of the charge carriers in the direction of the external applied

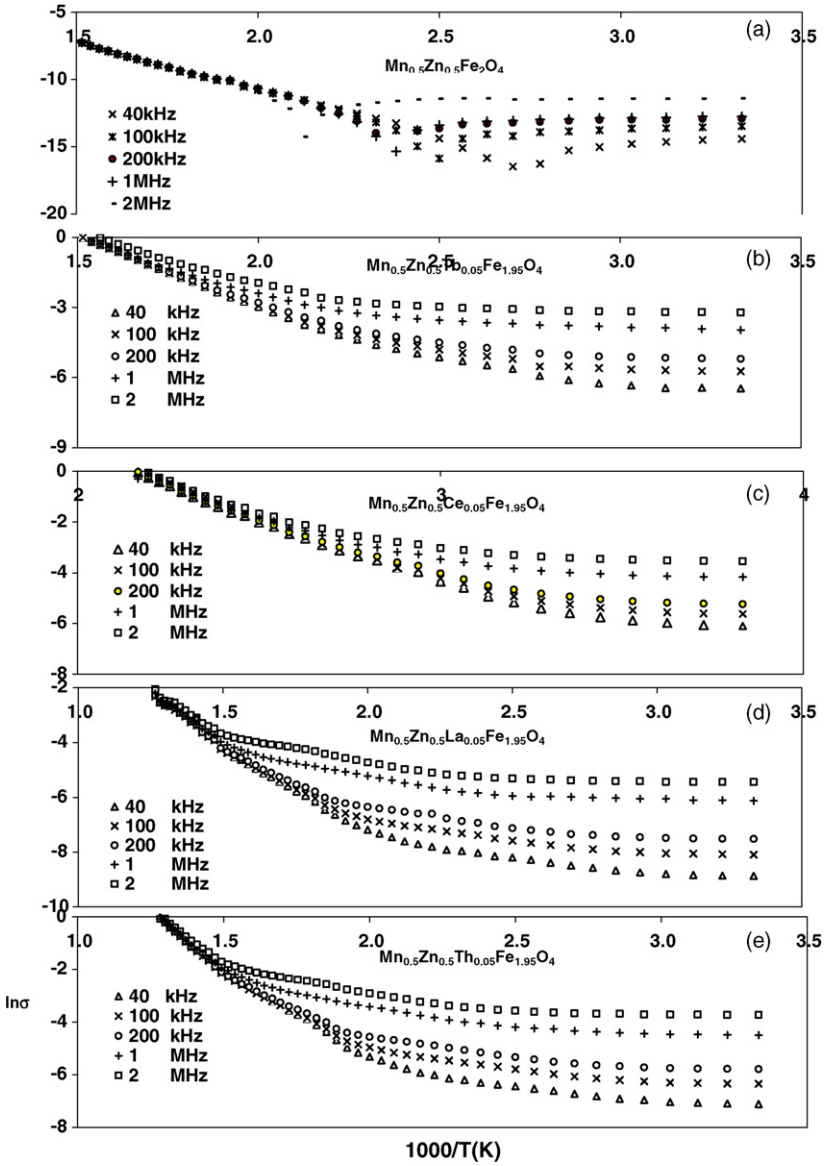

Fig. 7. (a–e) Correlation between the electrical conductivity ($\ln \sigma$) and reciprocal absolute temperature (T) for all investigated samples.

electric field, resulting from dielectric polarization process. In addition, all the rare-earth ions increase the electrical resistivity of Mn–Zn ferrite as a result of the formation of an insulating intergranular secondary phase ($RFeO_3$ contains Fe^{3+} ions only). But, at the same time, the crystallization of the secondary stable phase on the grain boundaries impedes the oxidation of Fe^{2+} ions inside the grains during the slow cooling of the samples. For this reason, there is a good correlation between the resistivity of the samples and Fe^{2+} ion concentration. The small value of electrical resistivity for Ce substitution may be attributed to Ce valence fluctuations between Ce^{3+} and Ce^{4+} ions which result from the strong hybridization between 4f and 3d conduction electrons [30,34]. Fig. 6d correlates the dependence of conductivity σ (σ at room temperature) on the ionic radius. From the figure it is clear that the value of σ decreases with increasing the ionic radius. As the ionic radius increases, the mobility and concentration of the charge carriers decreases, therefore the conductivity decreases.

Fig. 7a–e correlates the a.c. electrical resistivity ($\ln \sigma$) versus the reciprocal of the absolute temperature $1000/T$. From the obtained data, it is clear that the frequency dependence behavior in the ferrimagnetic region gives a metallic like behavior for all samples up to the Curie temperature T_C, while above T_C it becomes frequency independent (paramagnetic region). The slopes of these lines indicate that the exchange interaction between outer and inner electrons affects directly on the Curie temperature where the samples are transformed from ferrimagnetic (ordered state) to paramagnetic (disordered). The values of the activation energy in the two regions (ferrimagnetic and paramagnetic) are listed in Table 3.

Fig. 8a shows the relation between the dielectric constant ε' versus the frequency ($\ln f$) at a selected temperature 450 K. It is clear that the continuous decrease of ε' with increasing the frequency is acceptable. This is because the hopping process cannot match the field vibration which gives the local displacements of the electrons in the direction

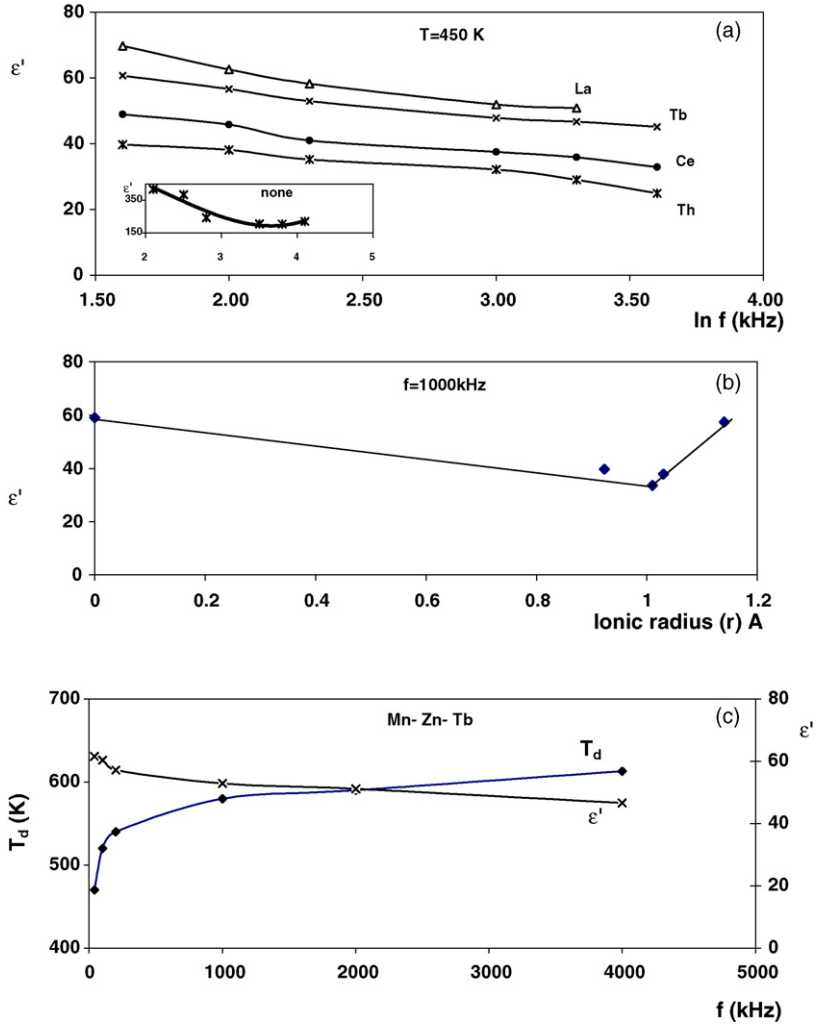

Fig. 8. (a–c) The change of dielectric constant ε' with different frequency ($\ln \sigma$). (b) Dependence of ε' on ionic radius of rare-earth ions. (c) Correlation between ε' and transition temperature (T_d) as a function of frequency.

Table 3
The activation energy in (eV) two regions E_1 and E_2 for different rare-earth ions of $Mn_{0.5}Zn_{0.5}R_{0.05}Fe_{1.95}O_4$

Sample	40 kHz		100 kHz		200 kHz		1000 kHz		2000 kHz	
	E_1	E_{11}	E_1	E_{11}	E_1	E_{11}	E_1	E_{11}	E_1	E_2
None	0.11	0.29	0.12	0.27	0.11	0.25	0.13	0.27	0.12	0.27
Tb	0.15	0.27	0.15	0.34	0.15	0.28	0.15	0.28	0.14	0.25
Ce	0.15	0.21	0.14	0.24	0.12	0.28	0.11	0.26	0.12	0.23
La	0.12	0.62	0.12	0.61	0.13	0.64	0.12	0.49	0.13	0.46
Th	0.11	0.41	0.11	0.39	0.27	0.39	0.27	0.46	0.17	0.46

of the applied electric field. The dielectric constant dependence on the ionic radius (r) of R^{3+} ions substituted is shown in Fig. 8b. It can be seen that ε' decreases with increasing r up to $r = 1.01$Å then it decreases, after which suddenly increases. This can be explained due to the electron exchange interaction which leads to polarization in ferrites where some of the rare-earth ions on the octahedral sites decrease the exchange interaction as $Fe^{2+} \leftrightarrow Fe^{3+}$ with the result of decreasing the polarization as well as the dielectric constant. Fig. 8c shows the effect of applied frequency on both dielectric constant ε' and transition temperature T_d. It can be seen that there is a pronounced low value of T_d at about 40 kHz after which a gradual increase at about 10^3 kHz then nearly steady state for higher frequencies is

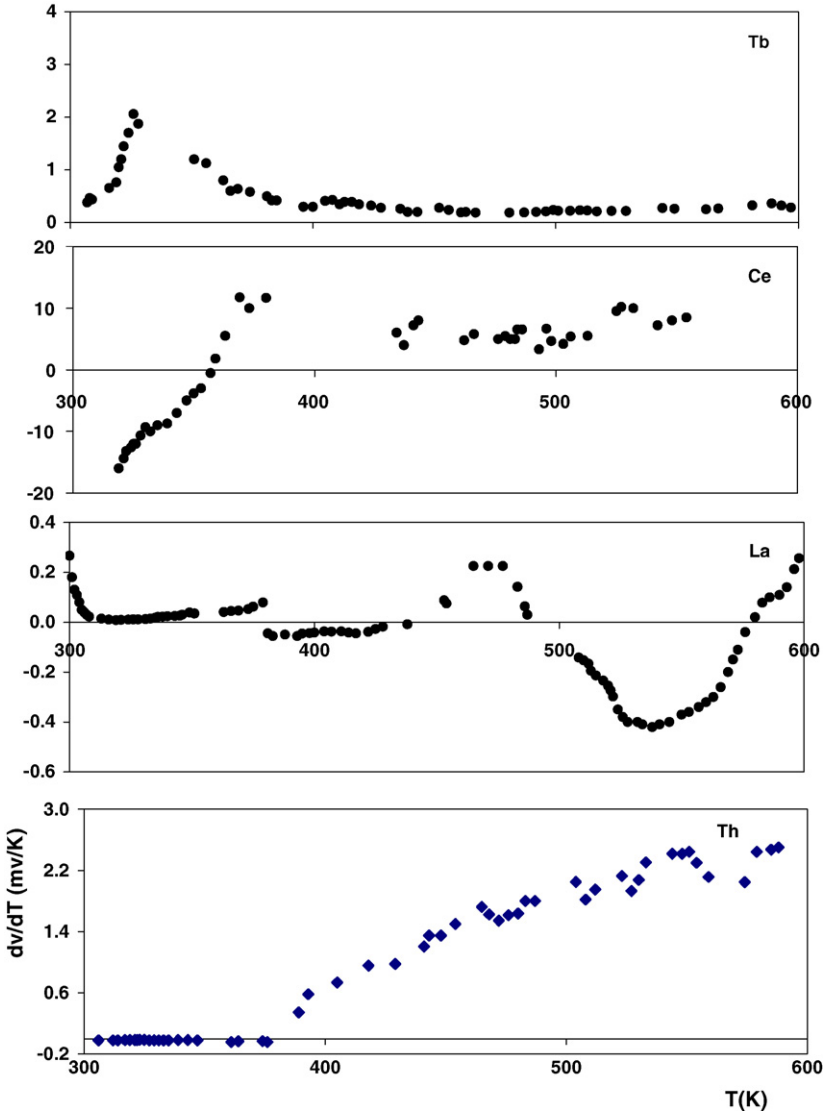

Fig. 9. Variation of Seebeck coefficient (S) with absolute temperature (T) for the rare-earth-substituted samples.

obtained. This behavior occurs because of the rapid electron exchange interaction between $Fe^{2+} \leftrightarrow Fe^{3+}$ with increasing frequency. While ε' is gradually decreased up to 200 kHz, and then gives nearly steady state for higher frequency.

3.4. Thermoelectric power

The p- or n-type nature of the charge carriers below and above the transition temperature was determined from the sign of Seebeck coefficient as in Fig. 9. It is clear that the variation in the charge carriers between n- or p-type is independent on R^{3+} type or size. The negative and positive values of thermoelectric power found over the entire temperature range studied shows that the majority of charge carriers are holes. On the basis of its positive sign, the above ferrites have been classified as p-type semiconductors. Thus, the conduction mechanism for p-type is predominant due to holes.

4. Conclusions

(1) The influence of the R ions on the electrical properties of Mn–Zn ferrite is explained as the effect of their ionic radius.
(2) The substitutions of iron ions by rare earth improved the magnetic susceptibility of the samples.
(3) From the viewpoint of effectiveness, the R^{3+} with a large radius and with a stable valence of 3+ is found to be the best substituents for improvements in the magnetic and electrical properties of the soft Mn–Zn ferrite.
(4) The small amount of R^{3+} ions incorporated in the ferrite favor the formation of the crystalline secondary phases associated with modifications in the electrical and magnetic properties.
(5) The relationship between $\ln \sigma$ and $(1/T)$ show two regions of different activation energies. The difference between the two activation energies in the low (E_1) and high (E_2) is due to the thermal activation of the carrier mobility at higher temperatures.

References

[1] D. Ihile, B. Lorenz, Philos. Mag. B 42 (1980) 337.
[2] M.A. Ahmed, E.H. El-Khawas, F.A. Radwan, J. Mater. Sci. 36 (2001) 5031.
[3] E.C. S Sncllling, Proceeding of the Fifth International Conference on Ferrites (ICF-5) India, 1989, p. 579.
[4] S.H. Chen, S.C. Chang, I.N. Lin, J. Magn. Magn. Mater. 209 (2000) 193.
[5] M. Schacfer, G. Dietzmann, H. Wirth, J. Magn. Magn. Mater. 101 (1991) 95.
[6] M. Rozman, M. Drofenik, J. Am. Ceram. Soc. 78 (9) (1995) 2449.
[7] R. Valenzuela, Magnetic Ceramics, Cambridge University Press, 1994
[8] S.A. Mazen, B.A. Sabrah, Thermochim. Acta 105 (1986) 1.
[9] Y. Miyahara, J. Phys. Soc. Jpn. 32 (1972) 629.
[10] A.M. Van Dippen, F.K. Lotgering, Physica 86–88 (B+C) (1977) 981.
[11] P.J. Phillips, T.E. Whall, V.A.M. Brabers, Philos. Mag. B 71 (1995) 23.
[12] A. Verma, T.C. Goel, R.G. Mendiratta, R.G. Gupla, J. Magn. Magn. Mater. 192 (1992) 271.
[13] E. Rezlescu, N. Rezlescu, P.D. Mangeron, L. Rezlescu, C. Pasxick, J. Phys. Stat. Sol. (a) 162 (1997) 673.
[14] N. Bogoroditzkll, V.V. Pasynkov, R.R. Basili, Yu.M. Volokobinskll, Sov. Phys. Doklady 10 (1965) 85.
[15] V.M. Talanov, Izv. Vuzov, Khimiya I Khim. Tekhnol, 12 (1978) 1395.
[16] G.I. Ciufarov, Y.P. Vorobiev, in: Fizicheskaya Khimiya Okislov metallov, Izd, Moscow, p. 135, 1981.
[17] A. Vasiliu, G.H. Maxim, M.L. Craus, E. Luca, J. Phys. Stat. Sol. (a) 13 (1972) 371.
[18] N. Rezlescu, E. Rezlescu, C. Pasnicu, M.L. Craus, J. Phys. Condens. Matter 6 (1994) 5707.
[19] R.V. Mangalaraja, S. Ananthakumar, P. Manohar, F.D. Gnanam, Ferrites, Proceedings of the Eight International Conference of ferrites (ICF8), Kyoto, Japan, 2000, p. 313.
[20] R.V. Mangalaraja, S. Ananthakumar, P. Manohar, F.D. Gnanam, M. Awano, J. Mater. Sci. Eng., (A) 367 (2004) 301.
[21] R.V. Mangalaraja, S. Ananthakumar, P. Manohar, F.D. Gnanam, J. Magn. Magn. Mater. 253 (2002) 56.
[22] K. Vijaya Kumar, D. Ravinder, Mater. Lett. 52 (2002) 166.
[23] S.H. Chen, S.C. Chang, I.N. Lin, J. Magn. Magn. Mater. 209 (2000) 193.
[24] R. Mathur, D.R. Sharma, S.R. Vadera, S.R. Gupta, B.B. Sharma, N. Kumar, J. Nanostruct. Mater. 11 (1999) 5.
[25] E. Rezlescu, N. Rezlescu, C. Pasxicu, M.L. Craus, P.D. Popa, J. Cryst. Res. Technol. 31 (1996) 313.
[26] L.A. Vladimirtseva, G.V. Sasaturation magnetizaiononor, V.A. Gorbatynk, Sov. Powder Metall. Met. Ceram. (U.S.A.) 12 (1973) 669.
[27] R. Krishnan, V. Cagan, IEEE Trans. Magn. MAG-7 (1971) 613.
[28] L.G. Van Uitert, J. Appl. Phys. 26 (1955) 1289.
[29] M. Singh, S.P. Sud, Mater. Sci. Eng. B: Solid State Mater. Adv. Technol. 83 (1–3) (2001) 180.
[30] A.K. Rastogi, G. Hilscher, E. Gratz, N. Pilmayr, J. Phys. 49 (1988) 277.
[31] L. John Berchmans, R. Kalai Selvan, P.N. Selva Kumar, C.O. Augustin, J. Magn. Magn. Mater. 279 (2004) 103–110.
[32] Y. Fukuda, S. Nagata, K. Echizenya, J. Magn. Magn. Mater. 279 (2004) 325.
[33] N.J. Vander Laag, M.D. Snel, P.C.M.M. Magusin, G. de With, J. Eur. Ceram. Soc. 24 (2004) 2417–2424.
[34] K. Vijay Kumar, A. Chandra Shekara Reddy, D. Ravinder, J. Magn. Magn. Mater. 263 (2003) 121.